Stimulated Brillouin Scattering Based Image-Reject Microwave Signal Harmonic Down-Converter

Kunpeng Zhai, Sha Zhu, *Member, IEEE*, and Ninghua Zhu, *Member, IEEE*

***Abstract*—We propose and demonstrate a photonic microwave signal harmonic down-converter with image rejection capability via stimulated Brillouin scattering (SBS). A dual-polarization dual-parallel Mach–Zehnder modulator (DP-DPMZM) is driven by a radio frequency/image (RF/IM) signal and a local oscillation (LO) signal to realize equivalent phase modulation and 4th-order double sideband modulation respectively. The optical carriers from the two arms of the DP-DPMZM can cancel out each other after polarization combining, thereby increasing the useful optical signal power in photodetection. Since the beating notes between the IM-modulated signals and LO-modulated 4th-order sidebands interfere destructively, the down-converted IM signals disappear naturally, which makes the down-converted image parts be suppressed in optical domain. By using an SBS-based dual-band microwave photonic filter to suppress the RF modulated -1st-order sideband and amplify the +1st-order sideband, destructive interference can be broken. Therefore, the RF signal over frequency range of 21-28 GHz can be down-converted to intermediate frequency (IF) band, and the image rejection ratio (IRR) can be also improved to more than 55 dB. Under -160 dBm/Hz noise floor, the SFDR is 105.1 dB·Hz$^{2/3}$.**

***Index Terms*—Microwave photonics, harmonic frequency down-conversion, image rejection.**

I. Introduction

FREQUENCY conversion technology occupies an important position in modern electrical systems, and can realize up-conversion or down-conversion of microwave signals [1], [2]. In radar systems, it is necessary to mix the received high-frequency echo signal with the local oscillator (LO) signal to realize frequency down-conversion at the receiver, so that low-speed electrical devices can be used for signal post-processing. Benefiting from the high frequency, large bandwidth, low loss, easy-reconfiguration, and anti-electromagnetic interference of microwave photonics, photonic assisted frequency converters have attracted lots of attentions [3], [4].

Simply, based on the single-sideband modulation of a dual-parallel Mach-Zehnder modulator (DPMZM), radio frequency (RF) signals can be down-converted to intermediate frequency (IF) band. However, the RF and LO signals needs to be combined and then sent to the input ports of the modulation, which may cause undesired intermodulation effects [5]. By using an optical filter to remove the -1st-order sidebands of the RF- and LO-modulated carrier suppressed double sideband optical signals, frequency down conversion can be realized [6]. Whereas, the used of optical filter may restrict the frequency range of the mixer. Frequency down conversion systems can also be achieved based on four-wave mixing (FWM) effect in a semiconductor optical amplifier (SOA) or high-order modulation of modulators, which can enable microwave down-conversion in the electrical domain with a low-frequency electrical LO [7], [8]. However, due to the existence of the image (IM) signal whose frequency is symmetrical to the RF signal with respect to the LO signal, the down-converted IF signals in above schemes not only contain the useful IF signal, but also have the undesired IM down-converted interference signal, which may lead to fuzzy frequency identification and even distortion of useful IF signal. In order to reduce the interference of IM signal, a Hartley structure is commonly used to introduce an additional 90° phase shift between two electrical or optical IM signals at the end of the mixing system [9], [10], [11]. In this way, the down-converted IM signals can be eliminated after interference cancellation. Brillouin carrier suppression technique can be used to achieve mixer using the SBS loss spectrum to suppress the carrier of optical signal [12], [13]. A straight-forward way to realize the mixer is setting the phase shift of the photonic microwave phase shifter [14]. The other approach for image rejection is based on a microwave photonic filter to select the desired signal and suppress the image [15]. However, since no gain is applied to the RF signal, the image rejection ratio (IRR) of these schemes is limited. It should be noted that for an image-reject frequency down-converter, a high-frequency LO signal source is always essential to achieve frequency down-conversion of high-frequency RF signals to an intermediate frequency band. Therefore, an image-reject harmonic frequency down-converter with high rejection ratio is urgently desired.

In this paper, we propose and experimentally demonstrate a photonic harmonic down-converter with high image rejection

Manuscript received 4 July 2022; revised 22 September 2022; accepted 1 October 2022. Date of publication 4 October 2022; date of current version 13 October 2022. This work was supported in part by the National Key R&D Program of China under Grants 2019YFB2203104 and 2020YFB2205801, in part by the Natural Science Foundation of China under Grants 61805231, 61835010, and 61620106013, in part by the High-End Talent Team Construction Plan of Beijing University of Technology, and in part by the Zhejiang Lab's International Talent Fund for Young Professionals. (*Corresponding authors: Sha Zhu; Ninghua Zhu.*)

Kunpeng Zhai is with the State Key Laboratory of Integrated Optoelectronics, Institute of Semiconductors, Chinese Academy of Sciences, Beijing 100083, China, and also with the University of Chinese Academy of Sciences, Beijing 100049, China (e-mail: kpzhai@semi.ac.cn).

Sha Zhu is with the College of Microelectronics, Faculty of Information Technology, Beijing University of Technology, Beijing 100124, China (e-mail: zhusha@bjut.edu.cn).

Ninghua Zhu is with the State Key Laboratory of Integrated Optoelectronics, Institute of Semiconductors, Chinese Academy of Sciences, Beijing 100083, China (e-mail: nhzhu@semi.ac.cn).

Digital Object Identifier 10.1109/JPHOT.2022.3211997

This work is licensed under a Creative Commons Attribution 4.0 License. For more information, see https://creativecommons.org/licenses/by/4.0/

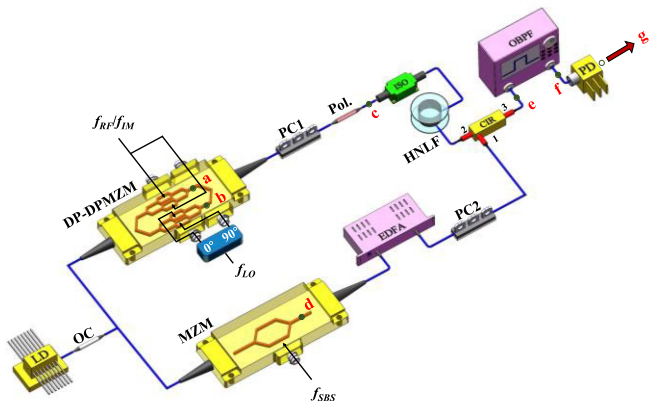

Fig. 1. Schematic diagram of the proposed photonic frequency down-converter.

ability based on stimulated Brillouin scattering (SBS). A RF/IM microwave signal and a LO signal is used to generate equivalent phase modulated optical signal and 4th-order optical sidebands respectively in a dual-polarization dual-parallel Mach–Zehnder modulator (DP-DPMZM). The gain spectrum and attenuation spectrum of a dual-pump SBS are respectively applied to the +1st and -1st-order optical sideband of the RF signals to realize the conversion from phase modulation to intensity modulation. Therefore, the RF signal can be down-converted to IF band after photodetection and the IRR can be increased due to the gain of the RF signal. The gain spectrum of the SBS pump signal amplify the +1st-order RF modulated optical sideband. After photodetection, the power of the corresponding IF signal will be improved accordingly. Therefore, the image rejection ratio can also be increased. For the IM signal, there is an equivalent phase modulation relationship between its sidebands and the LO optical signal used for down-conversion. The down-converted IM signals will interference cancellated, and the image rejection are achieved. Moreover, the 4th-order sidebands of LO signal are used to perform frequency conversion, which allows us to use a cost-effective low frequency LO source to construct a high-performance microwave photonic harmonic frequency down-converter.

II. Principle and Theory

The schematic diagram of the proposed scheme is shown in Fig. 1. The optical signal emitted from a laser diode (LD) is divided into two paths. The upper path is used to realize frequency conversion, while the lower path is used to generate dual-pump SBS signals. The DP-DPMZM in the upper path consists of two orthogonally polarized dual-parallel Mach-Zehnder modulators. The *x*-DPMZM consists of sub-MZM1 and sub-MZM2, the *y*-DPMZM consists of sub-MZM3 and sub-MZM4. As shown in Fig. 1, the *x*-DPMZM is driven by an RF and an IM signal. By biasing the two sub-MZMs and the main *x*-DPMZM at maximum, minimum, and maximum transmission points and applying Jacobi-Anger expansion, optical field at the output of

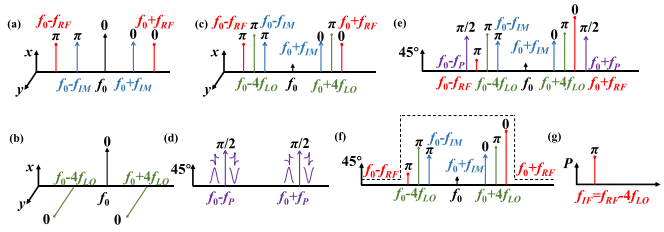

Fig. 2. Simplified optical or electrical spectra at different pots in Fig. 1.

the upper DPMZM can be written as

$$E_1(t) \propto \frac{1}{4} E_0 e^{j\omega_0 t} \cdot \times \begin{bmatrix} J_0(\beta_{RF}) + J_1(\beta_{RF})\, e^{j\omega_{RF} t} \\ -J_1(\beta_{RF})\, e^{-j\omega_{RF} t} + J_0(\beta_{IM}) \\ +J_1(\beta_{IM})\, e^{j\omega_{IM} t} - J_1(\beta_{IM})\, e^{-j\omega_{IM} t} \end{bmatrix}, \tag{1}$$

where ω_0 and E_0 are the angular frequency and amplitude of the optical carrier. $V_{RF}(t) = V_{RF}\cos(\omega_{RF}t)$, ω_{RF} and V_{RF} are the angular frequency and amplitude of the RF signal. $V_{IM}(t) = V_{IM}\cos(\omega_{IM}t)$ ω_{IM} and V_{IM} are the angular frequency and amplitude of the IM signal, $\beta_{RF} = \pi V_{RF}/V_\pi$ and $\beta_{IM} = \pi V_{IM}/V_\pi$ are the modulation index of the sub-MZMs, V_π is the half-wave voltage of the sub-MZMs, J_0 and J_1 are the zeroth- and first-order Bessel functions of the first kind. Therefore, the first-order RF and IM sidebands and optical carrier are generated as shown in Fig. 1(a).

Similarly, sub-MZM3 and sub-MZM4 are driven by a LO signal. The power of the LO signal is 10 dBm before sending to the modulator. Here, we used a 90° hybrid to realize optical carrier and 4th-order optical sideband modulation. A 90° hybrid is used to generate sine and cosine LO signals which are respectively loaded onto the two sub-MZMs of *y*-DPMZM. By setting the three direct current (DC) biases of the *y*-DPMZM as 0 V, the optical field at the output of the *y*-DPMZM can be given by

$$E_2(t) \propto \frac{1}{8} E_0 e^{j\omega_0 t} \cdot \begin{bmatrix} \left(e^{j\beta_{LO}\sin\omega_{LO}t} + e^{-j\beta_{LO}\sin\omega_{LO}t}\right) \\ +\left(e^{j\beta_{LO}\cos\omega_{LO}t} + e^{-j\beta_{LO}\cos\omega_{LO}t}\right) \end{bmatrix}$$
$$\propto \frac{1}{2} E_0 e^{j\omega_0 t} \cdot \begin{bmatrix} J_0(\beta_{LO}) + J_4(\beta_{LO})\, e^{j\cdot 4\omega_{LO}t} \\ +J_4(\beta_{LO})\, e^{-j\cdot 4\omega_{LO}t} \end{bmatrix}, \tag{2}$$

where $V_{LO}(t) = V_{LO}\sin(\omega_{RF}t)$, ω_{LO} and V_{LO} are the angular frequency and amplitude of the LO signal, $\beta_{\mathrm{LO}} = \pi V_{LO}/V_\pi$ is the modulation index of the sub-MZMs, J_4 is the 4th-order Bessel functions of the first kind. Therefore, a 4th-order double-sideband signal modulated by the LO signal is generated in the *y*-DPMZM, as shown in Fig. 2(b).

A polarization controller1 (PC1) and a polarizer (Pol.) are cascaded after the DP-DPMZM to realize polarization combination. The optical field after the Pol. can be expressed as

$$E_{Pol.}(t) = \cos\alpha_1 \cdot E_1(t) + \sin\alpha_1 \cdot E_2(t) e^{j\pi}, \tag{3}$$

where α_1 is the angle between the polarization direction of the Pol. and one principal axis of the polarization beam combiner (PBC), π phase shift between the two optical signals is

introduced by PC1. Under the condition of $\cos\alpha_1 \cdot 2[J_0(\beta_{RF}) + J_0(\beta_{IM})] = \sin\alpha_1 \cdot J_0(\beta_{LO})$, the optical carriers from the x-DPMZM and y-DPMZM can cancel out each other. Actually, a paralleled dual-parallel Mach–Zehnder modulator (DPMZM) is enough for our proposed mixer. With the development of the user defined integrated modulator chips, our system can get rid of the polarization sensitivity. Last and most important, based on the SBS effect, the proposed mixer can realize harmonic frequency down-conversion and high image-reject ratio as well as break the frequency limitation of most optical bandpass filter involved schemes simultaneously. In this context, the output optical signal of the Pol. is shown in Fig. 2(c) and given by

$$\begin{aligned} E_{Pol.}(t) \propto & \frac{1}{4}E_0 \cos\alpha_1 e^{j\omega_0 t} \\ & \times \begin{bmatrix} J_1(\beta_{RF})\, e^{j\omega_{RF}t} - J_1(\beta_{RF})\, e^{-j\omega_{RF}t} \\ +J_1(\beta_{IM})\, e^{j\omega_{IM}t} - J_1(\beta_{IM})\, e^{-j\omega_{IM}t} \end{bmatrix} \\ & + \frac{1}{2}E_0 \sin\alpha_1 e^{j\omega_0 t} \\ & \times \left[J_4(\beta_{LO})\, e^{j(4\omega_{LO}t+\pi)} + J_4(\beta_{LO})\, e^{-j(4\omega_{LO}t-\pi)} \right], \end{aligned} \tag{4}$$

In the lower dual-pump SBS signal generation path, a microwave signal is applied to the MZM. By biasing the MZM at its minimum transmission point, the output optical signal can be written as

$$E_{MZM}(t) \propto \frac{1}{2}E_0 e^{j\omega_c t} \begin{bmatrix} 2J_1(\beta_P)\, e^{j\left(-\omega_P t+\frac{\pi}{2}\right)} \\ +2J_1(\beta_P)\, e^{j\left(\omega_P t+\frac{\pi}{2}\right)} \end{bmatrix}, \tag{5}$$

where ω_P and V_P are the angular frequency and amplitude of the SBS pump signal, $\beta_{\rm P} = \pi V_P/V_\pi$ is the modulation index of the sub-MZMs, $f_{\rm p}$ is the frequency of the driven microwave signal. Thus, as shown in Fig. 2(d), a carrier-suppression double sideband (CS-DSB) modulated signal is generated. After being amplified by an erbium doped fiber amplifier (EDFA), the two optical sidebands are fed into the highly nonlinear optical fiber (HNLF) through a circulator (CIR) and act as dual-pump light to excite the SBS effect. By setting $f_{\rm p} = f_{\rm RF}+\nu_B$, where ν_B is the Brillouin frequency shift of the HNLF, the SBS-gain spectrum applies to the +1st-order optical sideband of RF-modulated signal, while the SBS-attenuation spectrum applies to the -1st-order optical sideband of RF-modulated signal, as illustrated in Fig. 2(e). The conversion from phase modulation to intensity modulation of RF signal can be achieved. The pump induced SBS gain factor g and loss factor α is described as

$$g(\Delta f_1) = \frac{g_0}{2}\frac{(\Gamma_B/2)^2}{\Delta f_1^2 + (\Gamma_B/2)^2} + j\frac{g_0}{4}\frac{\Gamma_B \Delta f_1}{\Delta f_1^2 + (\Gamma_B/2)^2}, \tag{6a}$$

$$\alpha(\Delta f_2) = -\frac{g_0}{2}\frac{(\Gamma_B/2)^2}{\Delta f_2^2 + (\Gamma_B/2)^2} - j\frac{g_0}{4}\frac{\Gamma_B \Delta f_2}{\Delta f_2^2 + (\Gamma_B/2)^2}, \tag{6b}$$

where g_0 and Γ_B are the line-center gain factor and Brillouin gain bandwidth of the HNLF respectively, $\Delta f_1 = |f\text{-}(f_0+f_p)|$ is the frequency deviation from (f_0+f_p), and $\Delta f_2 = |f\text{-}(f_0\text{-}f_p)|$ is the frequency deviation from $(f_0\text{-}f_p)$. We adjust the polarization

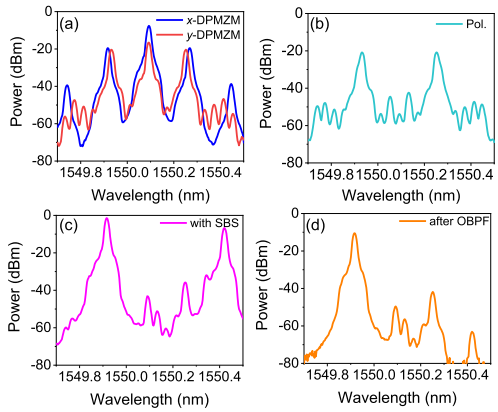

Fig. 3. Optical spectra of (a) at the output of DP-DPMZM, (b) after Pol., (c) after SBS process, and (d) after OBPF.

state of SBS pump path to make it be the same as that of upper path by PC2. As the optical signals propagate along the HNLF, the SBS process acts on the signal path. The peak in 1550.4 nm is an SBS noise which is resulted from the SBS gain spectrum of the -1st-order SBS pump signal, and it can be easily removed by the cascaded OBPF as shown in Figs. 2(f) and 3(d). When the optical signals are detected by a PD, the down converted IF signals are expressed as

$$\begin{aligned} I(t) \propto & \left\{ \begin{matrix} G(\Delta f_{RF}) \cdot J_1(\beta_{RF}) \cdot J_4(\beta_{LO}) \\ \times \cos\left[(\omega_{RF} - 4\omega_{LO})\, t\right] - \Phi(\Delta f_{RF}) \end{matrix} \right\} \\ & \times \frac{1}{8}E_0^2 \cos\alpha_1 \sin\alpha_1 \\ & - \left\{ \begin{matrix} A(\Delta f_{RF}) \cdot J_1(\beta_{RF}) \cdot J_4(\beta_{LO}) \\ \times \cos\left[(\omega_{RF} - 4\omega_{LO})\, t\right] + \Phi(\Delta f_{RF}) \end{matrix} \right\} \\ & \times \frac{1}{8}E_0^2 \cos\alpha_1 \sin\alpha_1, \end{aligned} \tag{7}$$

Due to the destructive interference between the two IM frequency down converted signals, the image rejection is achieved. The $G(\Delta f)$, $A(\Delta f)$, and $\Phi(\Delta f)$ is Eq. (8) are expressed as

$$G(\Delta f) = \exp\left\{ \frac{g_0 I_P L}{2} \frac{(\Gamma_B/2)^2}{\Delta f^2 + (\Gamma_B/2)^2} \right\}, \tag{8a}$$

$$A(\Delta f) = \exp\left\{ -\frac{g_0 I_P L}{2} \frac{(\Gamma_B/2)^2}{\Delta f^2 + (\Gamma_B/2)^2} \right\}, \tag{8b}$$

$$\Phi(\Delta f) = \frac{g_0 I_P L}{4} \frac{\Delta f \cdot \Gamma_B}{\Delta f^2 + (\Gamma_B/2)^2}, \tag{8c}$$

where L is the length of the HNLF, and I_P is the optical pump power injected into HNLF, $\Delta f_{\rm RF} = f_{\rm p}\text{-}\nu_{\rm B}\text{-}f_{\rm RF}$. Since $f_{\rm p} = f_{\rm RF}+\nu_B$, we can obtain $\Delta f_{\rm RF} = 0$, $\Phi(\Delta f_{\rm RF}) = 0$, $G(\Delta f_{\rm RF}) = G_{\max}$, $A(\Delta f_{\rm RF}) = A_{\min}$. The Eq. (7) can be rewritten as

$$\begin{aligned} I(t) \propto & \left\{ \begin{matrix} (G_{\max} - A_{\min}) \cdot J_1(\beta_{RF}) \cdot J_4(\beta_{LO}) \\ \times \cos\left[(\omega_{RF} - 4\omega_{LO})\, t\right] \end{matrix} \right\} \\ & \times \frac{1}{8}E_0^2 \cos\alpha_1 \sin\alpha_1, \end{aligned} \tag{9}$$

Thus, an image-reject harmonic frequency down-converter with high rejection ratio is realized.

III. Experimental Setup

A proof-of-concept experiment was constructed to verify the proposed harmonic down converter. A CW optical signal was divided into two parts, one part was fiber-coupled into a DP-DPMZM (Tektronix OM5110), the other part was launched into the MZM (iXblue MX-LN-40). A 5 dBm 22 GHz RF signal emitted by microwave source (Keysight N5 183B) was sent to the input ports of the *x*-DPMZM. As analyzed in theory, the DC biases of sub-MZM1, sub-MZM2 and main-*x*-DPMZM at set as 0 V, 3.5 V, and 0 V respectively. An equivalent phase modulated optical signal is shown in the blue line of Fig. 3(a). At the same time, a 5 GHz LO signal with power of 10 dBm was sent to a 90° electrical hybrid and then applied to the two microwave input ports of the *y*-DPMZM. By setting all the DC biases of sub-MZM3, sub-MZM4 and main-*y*-DPMZM at 0 V, optical carrier and 4th-order optical sideband modulation can be obtained in *y*-DPMZM. It should be noted that a four-channel RF amplifier is added before the modulator in Tektronix OM5110, so the microwave signal is amplified by a linear amplifier before being sent to the modulator, resulting in the high-order sideband power of LO signal. Moreover, when DPMZM realizes carrier suppression and ±4th-order sidebands modulation, the power of 4th-order sidebands is the sum of the 4th-order sidebands in sub-MZM3 and sub-MZM4. This will further increase the 4th-order LO signal power. The resolution of the OSA is 0.02 nm, which is difficult to distinguish the RF and LO signals in optical spectra. By adjusting the cascaded PC, the optical carriers can cancel out each other after polarization combination as illustrated in Fig. 3(b).

It is worth noting that, when any one of the modulation indices of the RF, IM and LO signals changes, we need to readjust PC1 according to the signal power to satisfy the cancellation conditions. Fortunately, the uncompleted suppressed optical carrier signal does not have much effect on the image-reject microwave signal harmonic down-converter, since the frequency of the beating signal between optical carrier and other sidebands is far from the desired frequency down-converted signal. Here we suppress the optical carrier to increase the useful power sent to the PD. In addition, for the polarization sensitivity, polarization-maintaining optical devices and polarization feedback controller can be used to control the polarization stability of the system in real-world application. The MZM in lower path is driven by an SBS pump microwave signal at frequency of 31.42 GHz.

By amplifying the power of the lower dual-pump stimulated Brillouin scattering (SBS) signal to 20 dBm and feeding it into the highly nonlinear optical fiber (HNLF) through a circulator (CIR), SBS effect can be stimulated in the upper path. The SBS gain spectrum and attenuation spectrum are also important for RF sideband amplification and suppression, which indirectly improves the power of down conversion signal. By biasing the MZM at minimum transmission point, a dual-pump SBS signal is generated. After being amplified by an EDFA (Keopsys CEFA-C-HG), the SBS pump signal injected into a spool of HNLF through an optical circulator to exceed the SBS effect. Fig. 3(c) shows the optical signal in upper path after being processed by SBS. Afterwards, an optical band pass filter (OBPF, Yenista OPTICS XTA-50/U) is used to remove the SBS pump signals and noise in the signal path and its passband bandwidth is wide. For most OBPF involved mixing schemes, the OBPF is used to suppress undesired signal optical sideband which is different from our system. Due to the slow rise and slow down edges of the OBPF, their low frequency operational range is limited. Fig. 3(d) shows the optical spectra of the filtered optical signals. By broadening the electrical pump signal, it is possible to obtain a wideband SBS spectral responses [16], [17], [18]. Therefore, if we can use an arbitrary waveform generator (AWG) to generate a wideband signal as the pump light for the SBS effect, a broadband optical gain and attenuation spectrum can be realized to process wideband signals.

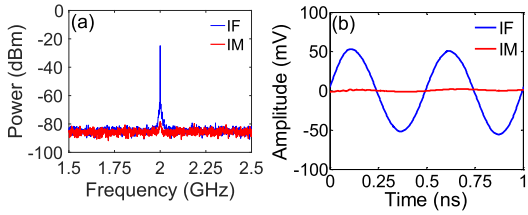

Fig. 4. (a) Electrical spectra of the down-converted IF signal and IM signal. (b) Waveforms of the down-converted IF signal and IM signal.

When the optical signals are detected by a PD (Optilab PD-40-M) and then shown in spectrum analyzer (Rohde&Schwarz FSW), the RF signal can be frequency down-converted to IF band. The blue lines in Fig. 4(a) and (b) shows the corresponding electrical spectrum and time-domain waveform of the obtained IF signal whose power is -26 dBm, frequency is 2 GHz and period is 0.5 ns. In order to verify the image rejection of the proposed mixer, the frequency of 22 GHz was adjusted to 18 GHz. The red line in Fig. 4(b) shows the electrical spectrum of the down-converted IM signal. The power is more than 55 dB lower than the desired IF signal. From the waveform of the red line in Fig. 4(b), it can be seen that the amplitude of the IM waveform is nearly 0 mV which agrees well the electrical spectrum.

Afterwards, the image rejection ability over a wide band is verified. First, we investigate the ability to down convert microwave signals from different frequency bands to the same IF frequency. The frequency of the RF signal is adjusted from 21 GHz to 28 GHz, while the LO signal frequency is changed from 4.75 GHz to 6.5 GHz accordingly. In our experiment, the bandwidth of the mixer is mainly limited by the used electrical 90° hybrid coupler which is 4.5 GHz-7 GHz. If an electrical 90° hybrid coupler with large bandwidth can be used, frequency range of the image-reject harmonic frequency down-converter can be improved a lot. Fig. 5 shows the electrical spectra of the frequency down-converted RF signals under the same IF frequency of 2 GHz. The power of the down-converted RF signal, as shown by the blue line in Fig. 6(a), is in the range of −23 to −26 dBm.

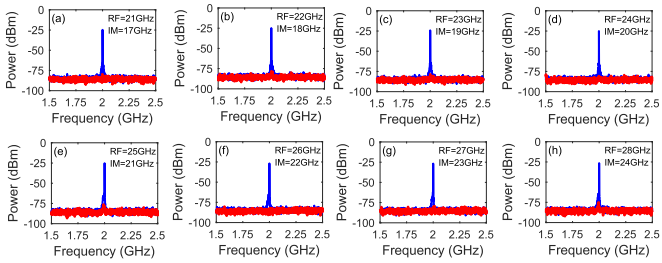

Fig. 5. Measured electrical spectra of the frequency down-converted RF and IM signals under the same IF frequency of 2 GHz.

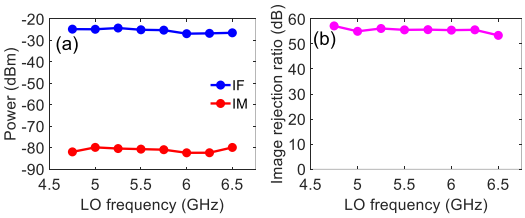

Fig. 6. (a) Power of the IF signals and IM signals. (b) Image rejection ratio of the frequency down converter.

TABLE I
PEFORMANCE COMPARATION

Ref.	IRR (dB)	SFDR (dB·Hz$^{2/3}$)	Gain (dB)	RF (GHz)	LO (GHz)	IF (GHz)
[9]	NA	108	-10	40	39.9	0.1
[11]	40	100.6	-50	33.000 25	30	3.0002 5
[13]	NA	93	-40	13	10.87	2.13
[14]	60	NA	NA	21	20	1
[15]	60	110	NA	12	11	1
Our work	55	105.1	-40	21	5	1

In order to check the image rejection, the frequency of the IM signal is tuned from 17–24 GHz. The measured electrical spectra and the power of the down-converted IM signals are shown in the red lines of Figs. 5 and 6(a). All powers are below -80 dBm. Fig. 6(b) shows the measured IRR of the frequency down converter. Benefiting the SBS effect, the IRRs are more than 55 dB.

Next, we kept the frequency of the LO signal at 5 GHz, while the frequencies of the RF and IM signals are changed from 21–28 GHz and 19–12 GHz to verify the tunability of the IF band. The 21–28 GHz RF signals are harmonic down-converted to 1–8 GHz using a 5 GHz LO signals. The IRRs of both the two situations are more than 55 dB. Fig. 7 shows the electrical spectra of the frequency IF signals under the same LO frequency of 5 GHz. The power of the down-converted RF signal, as shown by the blue line in Fig. 8(a), is in the range of −23 to −26 dBm. By tuning IM signals from 19–12 GHz, the image rejection was checked. The measured electrical spectra and the power of the down-converted IM signals are shown in the red lines of Figs. 7 and 8(a). All powers are below −80 dBm. Fig. 8(b) shows the measured IRR of the proposed frequency down converter. IRRs in excess of 55 dB can be obtained. The limited IRR can be

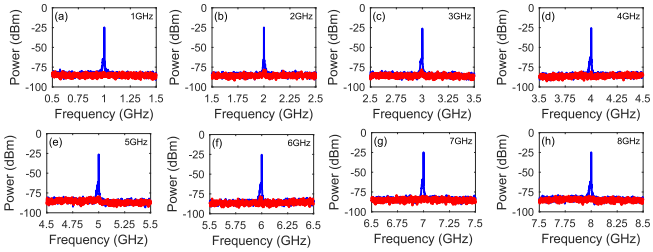

Fig. 7. Measured electrical spectra of the frequency down-converted RF and IM signals under the same LO frequency of 5 GHz.

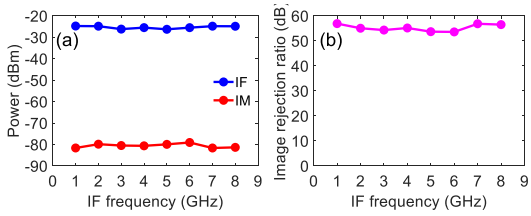

Fig. 8. (a) Power of IF signal and IM signal. (b) Image rejection ration of IF frequency.

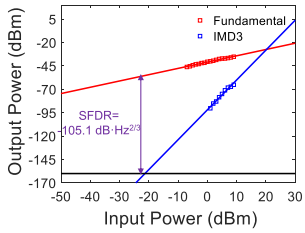

Fig. 9. Measured power of the fundamental and IMD3 of the output power.

attributed to the lower frequency down-converted RF signal power and the higher frequency down-converted IM signal power. First, from the optical spectrum of Fig. 3(c) and (d), it can be seen that the suppression ratio of the -1st-order RF-modulated optical signal is about 20 dB, that will decrease the power of the frequency down-converted RF signal. Second, the incomplete equivalent phase modulation of the IM signal caused by the DC bias errors and drifts is also an important reason, resulting in a down-converted IM signal, which also reduces the IRR. Thirdly, another reason for low IRR is the power of down-converted IF signal is relatively low. By increasing the input power of the RF and LO signal, the IRR can be further improved.

Finally, we measured the dynamic range of the proposed image rejected mixer. To measure the dynamic range, a two-tone signal with frequency of 22 GHz and 22.01 GHz are sent to the input of the DP-DPMZM. The LO signal is set as 5 GHz. Afterwards, the power of the desired 2 GHz and 2.01 GHz fundamental signals and undesired 1.99 GHz and 2.02 GHz IMD3 signals are measured by an electrical spectrum analyzer. After fitting the parameters as shown in Fig. 9, the SFDR can be obtained. The output power of the fundamental term and the third-order intermodulation distortions (IMD3) are shown in Fig. 9. The noise floor is at -160 dBm/Hz which is measured by electrical spectrum analyzer, and a spurious free dynamic

range (SFDR) of 105.1 dB·Hz$^{2/3}$ are obtained. The gain of the system is about −40 dB, because there is no built-in or external amplifier in PD, and EDFA is not added to the RF signal optical path. And we compare the performance of our mixer with other schemes in Table I. It shows that the frequency of the used LO signal for high frequency RF signal down-conversion in our system is much lower than other systems, which can decrease the high-frequency requirement of LO signal source.

IV. Conclusion

In this paper, a flexible photonic microwave image rejection harmonic down-converter based on SBS has been theoretically and experimentally demonstrated. A DP-DPMZM is driven by the RF/IM signal and LO signal to generate equivalent phase modulation. Based on the SBS effect, the proposed mixer can realize harmonic frequency down-conversion and high IRR, as well as break the frequency limitation of most optical bandpass filter involved schemes simultaneously. By adjusting the RF signals from 21 GHz to 28 GHz, the IF signals can be down converted to 2 GHz when the LO signals change from 4.75 GHz to 6.5 GHz, and the IF signals can also be down converted to 1-8 GHz when LO signals are fixed at 5 GHz. Experimental results exhibit an image rejection of larger than 55 dB, and the SFDR is 105.1 dB·Hz$^{2/3}$.

Acknowledgment

The authors declare no conflicts of interest.

References

[1] M. Celebiler and G. Stette, "On increasing the down-link capacity of a regenerative satellite repeater in point-to-point communications," *Proc. IEEE*, vol. 66, no. 1, pp. 98–100, Jan. 1978.

[2] J. D. Gayrard, "Evolution of telecommunication payloads: The necessity of new technologies," in *Proc. 20th AIAA Int. Commun. Satell. Syst. Conf. Exhibit.*, May 2002, Art. no. 1848.

[3] Z. S. Jia, J. J. Yu, and G. K. Chang, "All-optical 16/spl times/2.5 Gb/s WDM signal simultaneous up-conversion based on XPM in an NOLM in ROF systems," *IEEE Photon. Technol. Lett.*, vol. 17, no. 12, pp. 2724–2726, Dec. 2005.

[4] J. Yu, Z. Jia, L. Yi, and Y. Su, "Optical millimeter-wave generation or up-conversion using external modulators," *IEEE Photon. Technol. Lett.*, vol. 18, no. 1, pp. 265–267, Jan. 2006.

[5] Z. Tang and S. Pan, "A filter-free photonic microwave single sideband mixer," *IEEE Microw. Wireless Compon. Lett.*, vol. 26, no. 1, pp. 67–69, Jan. 2016.

[6] Y. Gao, A. Wen, Z. Tu, W. Zhang, and L. Lin, "Simultaneously photonic frequency down conversion, multichannel phase shifting, and IQ demodulation for wideband microwave signals," *Opt. Lett.*, vol. 41, no. 19, pp. 4484–4487, Oct. 2016.

[7] X. Zou et al., "Microwave photonic harmonic down-conversion based on cascaded four-wave mixing in a semiconductor optical amplifier," *IEEE Photon. J.*, vol. 10, no. 1, Feb. 2018, Art. no. 5500308.

[8] S. Zhu, M. Li, N. Zhu, and W. Li, "Photonic radio frequency self-interference cancellation and harmonic down-conversion for in-band full-duplex radio-over-fiber system," *IEEE Photon. J.*, vol. 11, no. 5, Oct. 2019, Art. no. 5503110.

[9] Y. Gao, A. Wen, W. Chen, and X. Li, "All-optical, ultra-wideband microwave I/Q mixer and image-reject frequency down-converter," *Opt. Lett.*, vol. 42, no. 6, pp. 1105–1108, Mar. 2017.

[10] Z. Shi, S. Zhu, M. Li, N. Zhu, and W. Li, "Reconfigurable microwave photonic mixer based on dual-polarization dual-parallel Mach–Zehnder modulator," *Opt. Commun.*, vol. 428, pp. 131–135, Jul. 2018.

[11] T. Lipkowitz, U. Horton, and E. Murphy, "Wideband microwave electro-optic image rejection mixer," *Opt. Lett.*, vol. 44, no. 19, pp. 4710–4713, Oct. 2019.

[12] E. H. W. Chan and R. A. Minasian, "High conversion efficiency microwave photonic mixer based on stimulated Brillouin scattering carrier suppression technique," *Opt. Lett.*, vol. 38, no. 24, pp. 5292–5295, Dec. 2013.

[13] M. Alom, S. Haxha, and A. Aggoun, "Photonic mixer incorporating all-optical microwave frequency generator based on stimulated Brillouin scattering using single laser source," *IEEE Access*, vol. 8, pp. 37045–37051, 2020.

[14] Z. Tang and S. Pan, "Image-reject mixer with large suppression of mixing spurs based on a photonic microwave phase shifter," *J. Lightw. Technol.*, vol. 34, no. 20, pp. 4729–4735, Oct. 2016.

[15] Y. Zhang et al., "Broadband image-reject mixing based on a polarization-modulated dual-channel photonic microwave phase shifter," *IEEE Photon. J.*, vol. 12, no. 2, Apr. 2020, Art. no. 7800409.

[16] G. Zoireff, D. Samaniego, and B. Vidal, "Dynamic filtering of microwave signals through Brillouin-based polarization-sensitive balanced detection," *IEEE J. Sel. Topics Quantum Electron.*, vol. 27, no. 2, Mar./Apr. 2021, Art. no. 7500206.

[17] A. Mahendra, Y. Liu, E. Magi, A. Choudhary, D. Marpaung, and B. Eggleton, "High link performance of Brillouin-loss based microwave bandpass photonic filters," *OSA Continuum*, vol. 1, no. 4, pp. 1287–1297, Dec. 2018.

[18] Y. Peled, M. Tur, and A. Zadok, "Generation and detection of ultra-wideband waveforms using stimulated Brillouin scattering amplified spontaneous emission," *IEEE Photon. Technol. Lett.*, vol. 22, no. 22, pp. 1692–1694, Nov. 2010.